

finite horizons. To facilitate defining LTL tasks over infinite horizons, recent works [26], [27] improve the results from [28] by converting LTL into a novel automaton, i.e., E-LDGBA, which is a variant of the Limit Deterministic Generalized Büchi Automaton (LDGBA) [29]. To improve the performance for the long-term (infinite horizons) satisfaction, they propose a modular architecture of Deep Deterministic Policy Gradient (DDPG) [4] to decompose the global missions into sub-tasks. However, none of the existing works can handle large-scale, complex environments, since an LTL-based reward requires the RL-agent to visit the regions of interest towards the LTL satisfaction. Consequently, such sparse rewards can not handle challenging environments. Applying sampling-based method or reachability control synthesis for LTL satisfaction is investigated in [30]–[33]. They all assume the known dynamic system. In contrast, our paper proposes a model-free approach for LTL-based navigation control in complex environments.

Contributions: Intuitively, the most effective way of addressing the environmental challenges of learning is optimizing the density of rewards to easily collect more effective data during learning such that the portion of transitions with positive rewards in the reply buffer is dramatically increased. To do so, we bridge the gap between sampling-based planning and model-free DPGs to solve standard reachability problems. In particular, our paper proposes an effective exploration guidance technique using geometric RRT* [13], to design the rewards. We extend such an innovation to propose a distributed sampling-based learning framework for LTL satisfaction in complex environments. In summary, the technical contributions of the paper are as follows:

- Our framework bridges actor-critic RL and RRT* methods and synthesizes model-free optimal policies over a continuous state-action space.
- We propose an automaton method to address the non-Markovian properties of reward design. Due to unknown dynamics, we overcome the infeasibility of the geometric RRT* guidance.
- We validate our algorithm through case studies to show its better performance compared to the distance and goal-oriented baselines. We show our method achieves significant improvements over exploration, concerning the environmental challenges.

II. PRELIMINARIES

The evolution of a continuous-time dynamic system \mathcal{S} starting from an initial state $s_0 \in S_0$ is given by

$$\dot{s} = f(s, a), \quad (1)$$

where $s \in S \subseteq \mathbb{R}^n$ is the state vector in the compact set S and $a \in A \subseteq \mathbb{R}^m$ is the control input. The functions $f : \mathbb{R}^n \times \mathbb{R}^m \rightarrow \mathbb{R}^n$ is locally Lipschitz continuous and unknown.

Consider a robot with the unknown dynamics \mathcal{S} in (1), operating in an environment Env that is represented by a compact subset $X \subset \mathbb{R}^d, d \in \{2, 3\}$ as a geometric space (workspace of the robot). The relation between \mathcal{S} and X is defined by the projection $Proj : S \rightarrow X$. The space X contains regions of interest that are labeled by a set of atomic

propositions AP , with the labeling function $L_X : X \rightarrow 2^{AP}$. Let $L : S \rightarrow 2^{AP}$ be a labeling function over S i.e., $L(s) = L_X(Proj(s))$.

Reinforcement Learning: The interactions between environment Env and the unknown dynamic system \mathcal{S} with the state-space S , can be captured by a continuous labeled-Markov Decision Processes (cl-MDP) [34]. A cl-MDP is a tuple $\mathcal{M} = (S, S_0, A, p_S, AP, L, R, \gamma)$, where $S \subseteq \mathbb{R}^n$ is the continuous state space, S_0 is the set of initial states, $A \subseteq \mathbb{R}^m$ is the continuous action space, p_S represents the unknown system dynamics as a distribution, AP is the set of atomic propositions, $L : S \rightarrow 2^{AP}$ is the labeling function, $R : S \times A \times S \rightarrow \mathbb{R}$ is the reward function, and $\gamma \in (0, 1)$ is the discount factor. The distribution $p_S : \mathfrak{B}(\mathbb{R}^n) \times A \times S \rightarrow [0, 1]$ is a Borel-measurable conditional transition kernel, s.t. $p_S(\cdot | s, a)$ is the probability measure of the next state given current $s \in S$ and $a \in A$ over the Borel space $(\mathbb{R}^n, \mathfrak{B}(\mathbb{R}^n))$, where $\mathfrak{B}(\mathbb{R}^n)$ is the set of all Borel sets on \mathbb{R}^n .

Let $\pi(a|s)$ denote a policy that is either deterministic, i.e., $\pi : S \rightarrow A$, or stochastic, i.e., $\pi : S \times A \rightarrow [0, 1]$, which maps states to distributions over actions. At each episode, the initial state of the robot in Env is denoted by $s_0 \in S_0$. At each time step t , the agent observes the state $s_t \in S$ and executes an action $a_t \in A$, according to the policy $\pi(a_t | s_t)$, and Env returns the next state s_{t+1} sampled from $p_S(s_{t+1} | s_t, a_t)$. The process is repeated until the episode is terminated. The objective of the robot is to learn an optimal policy $\pi^*(a|s)$ that maximizes the expected discounted return $J(\pi) = \mathbb{E}^\pi \left[\sum_{k=0}^{\infty} \gamma^k \cdot R(s_k, a_k, s_{k+1}) \right]$ under the policy π .

Linear Temporal Logic (LTL): LTL is a formal language to describe complex properties and high-level specifications of a system. The ingredients of an LTL formula are a set of atomic propositions, and combinations of Boolean and temporal operators. The syntax of LTL is defined as [18]

$$\phi := \text{true} \mid a \mid \phi_1 \wedge \phi_2 \mid \neg \phi_1 \mid \bigcirc \phi \mid \phi_1 \mathcal{U} \phi_2,$$

where $a \in AP$ is an atomic proposition, *true*, *negation* \neg , and *conjunction* \wedge are propositional logic operators, and *next* \bigcirc and *until* \mathcal{U} are temporal operators. Alongside the standard operators introduced above, other propositional logic operators, such as *false*, *disjunction* \vee , and *implication* \rightarrow , and temporal operators, such as *always* \square and *eventually* \diamond , are derived from the standard operators.

The semantics of an LTL formula are interpreted over words, where a word is an infinite sequence $o = o_0 o_1 \dots$, with $o_i \in 2^{AP}$ for all $i \geq 0$, and 2^{AP} represents the power set of AP . The satisfaction of an LTL formula ϕ by the word o is denoted by $o \models \phi$. For a infinite word o starting from the step 0, let $o(t), t \in \mathbb{N}$ denotes the value at step t , and $o[t:]$ denotes the word starting from step t . The semantics of LTL are defined as [18]:

$$\begin{aligned} o \models \pi &\Leftrightarrow \pi \in o(0) \\ o \models \phi_1 \wedge \phi_2 &\Leftrightarrow o \models \phi_1 \text{ and } o \models \phi_2 \\ o \models \neg \phi &\Leftrightarrow o \not\models \phi \\ o \models \bigcirc \phi &\Leftrightarrow o[1:] \models \phi \\ o \models \phi_1 \mathcal{U} \phi_2 &\Leftrightarrow \exists t \text{ s.t. } o[t:] \models \phi_2, \forall t' \in [0, t), o[t':] \models \phi_1 \end{aligned}$$

In this work, we restrict our attention to LTL formulas that exclude the *next* temporal operator, which is not meaningful for continuous state-action space [33], [35].

III. PROBLEM FORMULATION

Consider a cl-MDP $\mathcal{M} = (S, S_0, A, p_S, AP, L, R, \gamma)$. The induced path under a policy $\pi = \pi_0\pi_1\dots$ over \mathcal{M} is $s_\infty^\pi = s_0\dots s_i s_{i+1}\dots$, where $p_S(s_{i+1}|s_i, a_i) > 0$ if $\pi_i(a_i|s_i) > 0$. Let $L(s_\infty^\pi) = o_0o_1\dots$ be the sequence of labels associated with s_∞^π , such that $o_i = L(s_i), \forall i \in \{0, 1, 2, \dots\}$. We denote the satisfaction relation of the induced trace with ϕ by $L(s_\infty^\pi) \models \phi$. The probability of satisfying ϕ under the policy π , starting from an initial state $s_0 \in S_0$, is defined as

$$\Pr_M^\pi(\phi) = \Pr_M^\pi(L(s_\infty^\pi) \models \phi \mid s_\infty^\pi \in \mathcal{S}_\infty^\pi),$$

where \mathcal{S}_∞^π is the set of admissible paths from the initial state s_0 , under the policy π , and the detailed computation of $\Pr_M^\pi(\phi)$ can be found in [18]. The transition distributions p_S of \mathcal{M} are unknown due to the unknown dynamic \mathcal{S} , and DRL algorithms are employed to learn the optimal control policies.

In this paper, the cl-MDP \mathcal{M} captures the interactions between a complex environment Env with geometric space X , and an unknown dynamic system \mathcal{S} . Note that explicitly constructing a cl-MDP \mathcal{M} is impossible, due to the continuous state-action space. We track any cl-MDP \mathcal{M} on-the-fly (abstraction-free) using deep neural network, according to the evolution of the dynamic system \mathcal{S} operating in Env .

Problem 1. Consider a set of labeled goal regions in Env i.e., $AP_G = \{\mathcal{G}_1, \mathcal{G}_2, \dots\}$. The safety-critical task is expressed as $\phi = \Box\neg\mathcal{O} \wedge \phi_g$, where ϕ_g is a general LTL specification. The objective is to synthesize the optimal policy π^* of \mathcal{M} satisfying the task ϕ , i.e., $\Pr_M^\pi(\phi) > 0$.

Assumption 1. Let X_{free} denote the obstacle-free space. We assume that there exists at least one policy that drives the robot from initial states toward the regions of interest while always operating in X_{free} . This is reasonable since the assumption ensures the existence of policies satisfying a given valid LTL specification.

For Problem 1, typical learning-based algorithms only assign positive rewards when the robot reaches any goal region $X_{\mathcal{G}_i}$ toward the LTL satisfaction, resulting exploration issues of DRL rendered from the environmental challenge. This point is obvious even when considering the special case of goal-reaching tasks, i.e., $\phi_p = \Box\neg\mathcal{O} \wedge \diamond\mathcal{G}_i$.

Example 1. Consider an autonomous vehicle as an RL-agent with unknown dynamics that is tasked with specification ϕ , shown in Fig. 1 (a). For a goal-reaching task as a special LTL formula $\phi_p = \Box\neg\mathcal{O} \wedge \diamond\mathcal{G}_1$, if the RL-agent only receives a reward after reaching the goal region \mathcal{G}_1 , it will be hard to explore the effective data with positive rewards task using noisy policies during learning. Such a problem becomes more challenging, where a general LTL task e.g., $\phi = \Box\neg\mathcal{O} \wedge \Box((\diamond\mathcal{G}_1 \wedge \diamond(\mathcal{G}_2 \wedge \diamond\dots \wedge \diamond\mathcal{G}_4))$ is considered that requires the agent to safely visit regions $\mathcal{G}_1, \mathcal{G}_2, \mathcal{G}_3, \mathcal{G}_4$ sequentially infinitely many times.

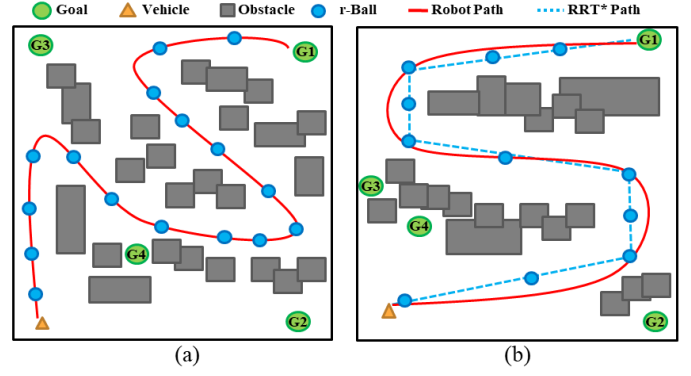


Fig. 1. Consider an autonomous vehicle operating in a complex and large-scale environment. It is challenging to learn optimal policies as described in Example 1. The trajectories provide insights of reward design in Section IV.

In the following, Section IV shows how to learn the control policy of completing one goal-reaching mission $\phi_p = \Box\neg\mathcal{O} \wedge \diamond\mathcal{G}_i$ in complex environments. Then, Section V presents how to decompose a general LTL task $\phi = \Box\neg\mathcal{O} \wedge \phi_g$ into a sequence of goal-reaching missions ϕ_p , which can be learned in a distributed manner in complex cluttered environments.

IV. OVERCOMING EXPLORATION

In Sec. IV-A, we briefly introduce the geometric sampling-based algorithm to generate an optimal path for the standard goal-reaching task $\phi_p = \Box\neg\mathcal{O} \wedge \diamond\mathcal{G}_i$. Based on that, Sec. IV-B develops a novel dense reward to overcome the exploration challenges and provides rigorous analysis for learning performance.

A. Geometric RRT*

The standard optimal RRT* method [13] is a variant of RRT [12]. Both RRT and RRT* are able to handle the path planning in complex and large-scale environments. Due to its optimality, we choose RRT* over RRT, to improve the learned performance of the optimal policies. Since the dynamic system \mathcal{S} is unknown, we use the geometric RRT* method that builds the tree $G = (V, E)$ incrementally in X , where V is the set of vertices and E is the set of edges. If V intersects the goal region, we find a geometric trajectory to complete the task ϕ . The detailed procedure of geometric RRT* is described in the Appendix A. Here, we briefly introduce two of the functions in the geometric RRT* method, which are used in explaining our method in the next sections.

Distance and cost: The function $dist : X \times X \rightarrow [0, \infty)$ is the metric that computes the geometric Euclidean distance between two states. The function $Cost : X \rightarrow [0, \infty)$ returns the length of the path in the tree between two input states.

Steering: Given two states x and x' , the function *Steer* returns a state x_{new} such that x_{new} lies on the geometric line connecting x to x' , and its distance from x is at most η , i.e., $dist(x, x') \leq \eta$, where η is a user-specified parameter. In addition, the state x_{new} must satisfy $dist(x_{new}, x') \leq dist(x, x')$.

Having the tree $G = (V, E)$ generated by the RRT* method, if there exists at least one node $x \in V$ that is located within the

goal regions, we find the optimal state trajectory satisfying the task ϕ as a sequence of geometric states $\mathbf{x}^* = x_0 x_1 \dots x_{N_p}$, where $x_{N_p} \in X_G$ and $x_i \in V, \forall i = 0, 1 \dots, N_p$.

B. Sampling-based reward

Here we use the optimal geometric trajectory \mathbf{x}^* and the properties of the generated tree $G = (V, E)$ to synthesize the reward scheme. First, let $x|\mathbf{x}^*$ denote a state of \mathbf{x}^* , and the total length of \mathbf{x}^* in the tree G be equal to $Cost(x_{N_p}|\mathbf{x}^*)$. We define the distance from each state $x \in \mathbf{x}^*$ to the destination x_{N_p} as $Dist(x|\mathbf{x}^*) = Cost(x_{N_p}|\mathbf{x}^*) - Cost(x|\mathbf{x}^*)$. Based on the distance, we design the RRT* reward scheme to guide the learning progress towards the satisfaction of ϕ . Passing an exact state in the continuous state space is challenging for robots. We define the norm r-ball for each state $x|\mathbf{x}^*$ to allow the robot passing the neighboring area of the state as $Ball_r(x|\mathbf{x}^*) = \{x' \in X \mid dist(x|\mathbf{x}^*, x') \leq r\}$, where $x|\mathbf{x}^*$ is the center and r is the radius. For simplicity, we select $r \leq \frac{\eta}{2}$ based on the steering function of the geometric RRT*, such that the adjacent r-balls along the optimal trajectory \mathbf{x}^* do not intersect with each other.

We develop a progression function $D : X \rightarrow [0, \infty)$ to track whether the current state is getting closer to the goal region, by following the sequence of balls along \mathbf{x}^* as:

$$D(x) = \begin{cases} Dist(x_i|\mathbf{x}^*) & \text{if } x \in Ball_r(x_i|\mathbf{x}^*) \\ \infty & \text{otherwise} \end{cases} \quad (2)$$

For the cl-MDP \mathcal{M} capturing the interactions between \mathcal{S} and \mathcal{Env} , the intuitive of the sampling-based reward design is to assign a positive reward whenever the robot gets geometrically closer to the goal region, along the optimal path obtained by the RRT* (Alg. 2).

During each episode of learning, a state-action sequence $s_0 a_0 s_1 a_1 \dots s_t$ up to current time t is projected into the state and action sequences $\mathbf{s}_t = s_0 s_1 \dots s_t$ and $\mathbf{a}_t = a_0 a_1 \dots a_{t-1}$, respectively. We define

$$D_{min}(\mathbf{s}_t) = \min_{s \in \mathbf{s}_t} \{D(Proj(s))\}$$

as the progression energy that is equal to the minimum distance along the optimal path towards the destination, up to step t . The objective of the reward is to drive the robot such that $D_{min}(\mathbf{s}_t)$ keeps dropping. However, employing the function $D_{min}(\mathbf{s}_t)$ for reward design that depends on the history of the trajectory results in a non-Markovian reward function [19], while the policy $\pi(s)$ only takes the current state as the input, and can not distinguish the progress achieved by the histories \mathbf{s}_t .

To address the issue, inspired by the product MPD [18], given the history \mathbf{s}_t , we keep tracking the index $i_t \in \{0, 1 \dots, N_p\}$ of the center state of the visited r-ball regions $Ball_r(x_{i_t}|\mathbf{x}^*)$ with minimum distance $Dist(x_{i_t}|\mathbf{x}^*)$ deterministically, i.e.,

$$x_{i_t} = Proj(s_{i_t}), \text{ where } s_{i_t} = \arg \min_{s \in \mathbf{s}_t} \{D(Proj(s))\}$$

If none of the r-balls are visited up to t , we set $i_t = 0$. Then, the current state s_t is embedded with the index i_t as a product state $s_t^\times = (s_t, i_t)$, which is considered as the input

of the policy, i.e., $\pi(s_t^\times)$. Note that we treat the embedded component i_t as the state of a deterministic automaton [18]. The relevant analysis can be found in Appendix B.

Let $R : s^\times \rightarrow \mathbb{R}$ denote the episodic reward function. We propose a novel scheme to assign the Markovian reward with respect to the product state s_t^\times as:

$$R(s_t^\times) = \begin{cases} R_-, & \text{if } Proj(s_t) \in X_O, \\ R_{++}, & \text{if } D(Proj(s_t)) = 0, \\ R_+, & \text{if } D(Proj(s_t)) < D_{min}(\mathbf{s}_{t-1}), \\ 0, & \text{otherwise,} \end{cases} \quad (3)$$

where R_+ is a positive constant reward, R_{++} is a boosted positive constant that is awarded when the robot reaches the destination, and R_- is the negative constant reward that is assigned when the robot violates the safety task of ϕ , i.e., $\phi_{safe} = \square \neg O$. Note that if the robot crosses both obstacles and r-balls, it receives the negative reward R_- , which has the first priority. This setting does not restrict selections of the parameter r (radius of r-balls) for implementations.

Example 2. As shown in Fig. 1 (a), we apply the RRT* method to generate the optimal trajectory (colored gray) in a challenging environment. Then, we construct the sequence of r-balls along it and apply the reward design (3) to guide the learning and overcome exploration.

Remark 1. Since geometric RRT* does not consider the dynamic system, the optimal path \mathbf{x}^* may be infeasible for the robot to follow exactly, with respect to any policy. As a running example in Fig. 1 (b), our RRT* reward is robust such that the robot is not required to strictly follow all r-balls of the optimal path. Instead, in order to receive the positive reward, the robot only needs to move towards the destination and pass **partial of** \rightarrow **through** the r-balls $Ball_r(x_i|\mathbf{x}^*), i \in \{0, 1 \dots, N_p\}$ along the optimal path.

By applying the reward design (3), we formally verify the performance of the reward (3) for the reach-avoid task ϕ_p as:

Theorem 1. *If Assumption 1 holds, by selecting R_{++} to be sufficiently larger than R_+ , i.e., $R_{++} \gg R_+$, any algorithm that optimizes the expected return $J(\pi)$ is guaranteed to find the optimal policy π^* satisfying the goal-reaching task ϕ_p , i.e., $\Pr_M^{\pi^*}(\phi_p) > 0$.*

The proof is presented in Appendix C. Theorem 1 provides a theoretical guarantee for the optimization performance, allowing us to apply practical algorithms to find the approximated optimal policy in continuous space.

Based on Theorem 1 and regarding the continuous control task, we apply advanced DRL methods, e.g., actor-critic algorithms [4], [5], [7], to find the optimal policy π^* . Consider a policy $\pi_\theta(a|s^\times)$, parameterized by θ , the learning objective aims to find the optimal policy via optimizing the parameters θ and maximizing the expected discount return $J(\theta) = \mathbb{E}^{\pi_\theta} \left[\sum_{t=0}^{\infty} \gamma^t \cdot R(s_t^\times) \right]$, which minimizes the loss function:

$$\mathcal{L}(\theta) = \mathbb{E}_{(s^\times, a, r, s'^\times) \sim \mathcal{D}} [(Q(s, a|\omega) - y)^2], \quad (4)$$

where \mathcal{D} is the replay buffer that stores experience tuples $(s^\times, a, R, s'^\times)$, $Q(s, a|\omega)$ is the state-action valuation function

parameterized by ω , and $y = r + \gamma Q(s'^{\times}, a'|\omega)$. As observed in (4), actor-critics rely on effective data in the replay buffer, or sample efficiency of the state distribution to minimize the loss function. Due to its high reward density over geometric space, the sampling-based reward is easy to explore and improves the training performance using noisy policies.

Theorem 2. *If Assumption 1 holds, by selecting R_{++} to be sufficiently larger than R_+ , i.e., $R_{++} \gg R_+$, a suitable DPG algorithm that optimizes the expected return $J(\theta)$, finds the optimal parameterized policy π_{θ}^* satisfying the LTL tasks ϕ_p , i.e., $\Pr_M^{\pi_M^*}(\phi_p) > 0$ in the limit.*

Theorem 2 is an immediate result of Theorem 1 and the nature of nonlinear regressions in deep neural networks. In practice, the number of episodes and steps are limited and training has to be stopped eventually.

V. LTL TASK SATISFACTION

Sec. V-A describes how to generate and decompose the optimal path of satisfying general LTL task ϕ in a sequence of paths of completing goal-reaching missions ϕ_p , and Sec. V-B explains how to integrate distributed DPGs with the novel exploration guidance of Sec. IV, to learn the optimal policy.

A. Geometric TL-RRT*

Due to the unknown dynamic system, we define the transition system over the geometric space X , referred as Geometric-Weighted Transition System (G-WTS).

Definition 1. A G-WTS of Env is a tuple $\mathcal{T} = (X, x_0, \rightarrow_{\mathcal{T}}, AP, L_X, C_{\mathcal{T}})$, where X is the geometric space of Env , x_0 is the initial state of robot; $\rightarrow_{\mathcal{T}} \subseteq X \times X$ is the geometric transition relation s.t. $x \rightarrow_{\mathcal{T}} x'$ if $dist(x, x') \leq \eta$ and the straight line σ connecting x to x_{new} is collision-free, AP is the set of atomic propositions as the labels of regions, $L_X : X \rightarrow AP$ is the labeling function that returns an atomic proposition satisfied at a location x , and $C_{\mathcal{T}} : (\rightarrow_{\mathcal{T}}) \rightarrow \mathbb{R}^+$ is the geometric Euclidean distance, i.e., $C_{\mathcal{T}}(x, x') = dist(x, x'), \forall (x, x') \in \rightarrow_{\mathcal{T}}$.

The standard WTS [33], [35] defines the transition relations $x \rightarrow_{\mathcal{T}} x'$ according to the existence of model-based controllers that drive the robot between neighbor regions x, x' . Differently, we only consider the geometric connection among states in a model-free manner.

Let $\tau_{\mathcal{T}} = x_0 x_1 x_3 \dots$ denote a valid run of \mathcal{T} . An LTL formula ϕ can be converted into a Non-deterministic Büchi Automata (NBA) to verify its satisfaction.

Definition 2. [36] An NBA over 2^{AP} is a tuple $\mathcal{B} = (Q, Q_0, \Sigma, \rightarrow_{\mathcal{B}}, Q_F)$, where Q is the set of states, $Q_0 \subseteq Q$ is the set of initial states, $\Sigma = 2^{AP}$ is the finite alphabet, $\rightarrow_{\mathcal{B}} \subseteq Q \times \Sigma \times Q$ is the transition relation, and $Q_F \subseteq Q$ is the set of accepting states.

A valid infinite run $\tau_{\mathcal{B}} = q_0 q_1 q_2 \dots$ of \mathcal{B} is called accepting, if it intersects with Q_F infinite often. Infinite words $\tau_o = o_0 o_1 o_2 \dots, \forall o \in 2^{AP}$ generated from an accepting run satisfy the corresponding LTL formula ϕ . An LTL formula is converted

into NBA using the tool [37]. As in [31], we prune the infeasible transitions of the resulting NBA to obtain the truncated NBA.

Definition 3. Given the G-WTS \mathcal{T} and the NBA \mathcal{B} , the product Büchi automaton (PBA) is a tuple $P = \mathcal{T} \times \mathcal{B} = (Q_P, Q_P^0, \rightarrow_P, Q_P^F, C_P, L_P)$, where $Q_P = X \times Q$ is the set of infinite product states, $Q_P^0 = x_0 \times Q$ is the set of initial states; $\rightarrow_P \subseteq Q_P \times 2^{AP} \times Q_P$ is the transition relation defined by the rule: $\frac{x \rightarrow_{\mathcal{T}} x' \wedge q \xrightarrow{L_X(x)} q'}{q_P = (x, q) \rightarrow_P q'_P = (x', q')}$, where $q_P \rightarrow_P q'_P$ denotes the transition $(q_P, q'_P) \in \rightarrow_P$, $Q_P^F = X \times Q_F$ is the set of accepting states, $C_P : (\rightarrow_P) \rightarrow \mathbb{R}^+$ is the cost function defined as the cost in the geometric space, e.g., $C_P(q_P = (x, q), q'_P = (x', q')) = C_{\mathcal{T}}(x, x'), \forall (q_P, q'_P) \in \rightarrow_P$, and $L_P : Q_P \rightarrow AP$ is the labelling function s.t. $L_P(q_P) = L_X(x), \forall q_P = (x, q)$.

A valid trace $\tau_P = q_P^0 q_P^1 q_P^2 \dots$ of a PBA is called accepting, if it visits Q_P^F infinitely often, referred as the acceptance condition. Its accepting words $\tau_o = o_0 o_1 o_2 \dots, \forall o_i = L_P(q_P^i)$ satisfy the corresponding LTL formula ϕ . Let τ_F denote an accepting trace, and $proj|_X : Q_P \rightarrow X$ is a function that projects product state space into the workspace, i.e., $proj|_X(q_P) = x, \forall q_P = (x, q)$. Using the projection, we extract the geometric trajectory $\tau_{\mathcal{T}} = proj|_X(\tau_F)$ that satisfies the LTL formula. More details are presented in [18]. Therefore, the planning objective is to find an acceptable path τ_P of PBA, with minimum accumulative geometric cost C_P .

However, the state space of G-WTS and PBA are both infinite. Consequently, we are not able to apply a graph search method to a PBA with infinite states. Thanks to the TL-RRT* algorithm [33] for providing an abstraction-free method, it allows us to incrementally build trees that explore the product state-space and find the feasible optimal accepting path. The procedure applies the sampling-based method over the PBA, and is inspired by the fact that the accepting run τ_F admits a lasso-type sequence in the form of prefix-suffix structure, i.e. $\tau_F = \tau_P^{pre} [\tau_P^{suf}]^{\omega}$, where the prefix part $\tau_P^{pre} = q_P^0 q_P^1 \dots q_P^K$ is only executed once, and the suffix part $\tau_P^{suf} = q_P^K q_P^{K+1} \dots q_P^{K+M}$ with $q_P^K = q_P^{K+M}$ is executed infinitely often.

Following this idea, we build the trees for the prefix and suffix paths, respectively. To satisfy the acceptance condition, the set of goal states of the prefix tree $G_P^{pre} = (V_P^{pre}, E_P^{pre})$ is defined as $Q_{goal}^{pre} = \{q_P = (x, q) \in X_{free} \times Q \subseteq Q_P \mid q \in Q_F\}$, where X_{free} is the collision-free geometric space. After obtaining the prefix tree, we construct the set $Q_{goal}^* = V_P^{pre} \cap Q_{goal}^{pre}$, and compute the optimal prefix path τ_{pre}^* reaching a state $q_P^* \in Q_{goal}^*$ from the root q_P^0 . The suffix tree $G_P^{suf} = (V_P^{suf}, E_P^{suf})$ is built by treating $q_P^* = (x^*, q^*)$ as the root, and its goal states are:

$$Q_{goal}^{suf}(q_P^*) = \{q_P = (x, q) \in X_{free} \times Q \subseteq Q_P \mid x \rightarrow_{\mathcal{T}} x^* \wedge q \xrightarrow{L_X(x)} q^*\}.$$

$Q_{goal}^{suf}(q_P^*)$ collects all states that can reach the state q_P^* via one transition, and this way it ensures the feasible cyclic path matching the suffix structure. Finally, we search the optimal suffix path τ_{suf}^* , by constructing $V_P^{suf} \cap Q_{goal}^{suf}$.

Algorithm 1 LTL-RRT*-Distributed DPGs

- 1: **Input:** Env , $\phi = \square \neg \mathcal{O} \wedge \phi_g$, Black-box \mathcal{S} ;
- 2: **Initialize:** Geometric space X , Primitives of TL-RRT*;
- 3: Convert ϕ into NBA \mathcal{B}
- 4: Build the incremental trees for PBA geometrically, based on definition 1 and definition 3
- 5: Generate the optimal trajectory $\tau_F^* = \tau_{pre}^*[\tau_{suf}^*]^\omega$
- 6: Reformulate the trajectory into the modular form

$$\mathcal{R}_F = (\mathcal{R}_0 \mathcal{R}_1 \dots \mathcal{R}_K)(\mathcal{R}_{K+1} \dots \mathcal{R}_{K+l})^\omega \quad (5)$$

- 7: **for** $i = 1, \dots, K + l$ **do**
- 8: Construct the RRT* reward based on (3) for \mathcal{R}_i
- 9: Assign an actor-critic DPG e.g., DDPG, PPO, for \mathcal{R}_i
- 10: **end for**
- 11: Assign the rewards (3) and DPGs for each \mathcal{R}_i .
- 12: Train the distributed DPGs in parallel
- 13: Extract the optimal policy π_i^* from each DPG \mathcal{R}_i
- 14: Concatenate all optimal policies in the form

$$\pi_\theta^* = (\pi_0^* \pi_1^* \dots \pi_K^*)(\pi_{K+1}^* \dots \pi_{K+l}^*)^\omega \quad (6)$$

B. Distributed DPGs

In this section, we first employ the optimal geometric path $\tau_F^* = \tau_{pre}^*[\tau_{suf}^*]^\omega$ from Section IV-A, to propose a distributed reward scheme. Since the policy gradient strategy suffers from the variance issue and only finds the optimal policy in the limit (see Theorem 2), instead of directly applying the reward design (3) for the whole path τ_F^* , we decompose it into sub-tasks. To do so, we modularly divide τ_F^* into separated consecutive segments, each of which shares the same automaton components, i.e., $\tau_F^* = \tau_0^* \tau_1^* \dots \tau_K^*[\tau_{K+1}^* \dots \tau_{K+l}^*]^\omega$ such that all states of each sub trajectory τ_i^* have the same automaton components. Each segment can be treated as a collision-free goal-reaching problem, denoted as $\mathcal{R}_i(\mathcal{G}_i, \mathcal{O})$, where \mathcal{G}_i is label of the i^{th} goal region. Specifically, suppose the state trajectory of each $\mathcal{R}_i(\mathcal{G}_i, \mathcal{O})$ is $\tau_i^* = q_{P,i}^0 q_{P,i}^1 \dots q_{P,i}^{N_i}$, we select the region labeled as $L_P(q_{P,i}^{N_i})$ containing the geometric state $proj|_X(q_{P,i}^{N_i})$.

We show an example of the optimal decomposition in Fig. 2, where the LTL task $\phi_{1,inf} = \square \neg \mathcal{O} \wedge \phi_{g_1}$ over infinite horizons with $\phi_{g_1} = \square \diamond \mathcal{G}_1 \wedge \square \diamond \mathcal{G}_2 \wedge \square \diamond \mathcal{G}_3$ that requires to infinitely visit goal regions labeled as $\mathcal{G}_1, \mathcal{G}_2, \mathcal{G}_3$. The resulting truncated NBA and decomposed trajectories of TL-RRT* are shown in Fig. 2 (a) and (b), respectively, where decomposed sub-paths are expressed as $\mathcal{R}_F = \mathcal{R}_{red}(\mathcal{R}_{blue} \mathcal{R}_{pink} \mathcal{R}_{brown})^\omega$, such that the distributed DPGs are applied to train the optimal sub-policies for each one in parallel.

The lasso-type optimal trajectory is reformulated as: $\mathcal{R}_F = (\mathcal{R}_0 \mathcal{R}_1 \dots \mathcal{R}_K)(\mathcal{R}_{K+1} \dots \mathcal{R}_{K+l})^\omega$. For the cl-MDP \mathcal{M} , we treat each \mathcal{R}_i as a task $\phi_{\mathcal{R}_i} = \square \neg \mathcal{O} \wedge \diamond \mathcal{G}_i$ solved in Section IV-B. In particular, we propose collaborative team of RRT* rewards in (3) for each sub-task and assign distributed DPGs for each \mathcal{R}_i that are trained in parallel. After training, we extract the concatenate policy π_i^* of each \mathcal{R}_i to obtain the global optimal policy as $\pi_\theta^* = (\pi_0^* \pi_1^* \dots \pi_K^*)(\pi_{K+1}^* \dots \pi_{K+l}^*)^\omega$. The overall procedure is summarized in Alg. 1, and a detailed

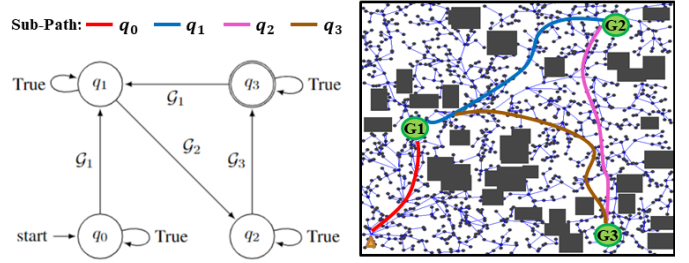


Fig. 2. Decomposition example. (Left) Truncated NBA \mathcal{B} of the LTL formula $\phi_{g_1} = \square \diamond \mathcal{G}_1 \wedge \square \diamond \mathcal{G}_2 \wedge \square \diamond \mathcal{G}_3$ for $\phi_{1,inf} = \square \neg \mathcal{O} \wedge \phi_{g_1}$; (Right) Decomposed sub goal-reaching tasks.

diagram with rigorous analysis is presented in Appendix D. Based on the decomposition properties and Theorem 2, we can conclude that the concatenated optimal policy of Alg. 1 satisfying the global LTL specification.

VI. EXPERIMENTAL RESULTS

We evaluate the framework by applying the framework on different nonlinear dynamic systems, to satisfy various LTL tasks. The algorithm test focuses on large-scale complex environments that generalize the simple ones to demonstrate their performance, where dense cluttered obstacles are randomly sampled. We integrate all baselines with either DDPG or SAC as DPG algorithms. Finally, we show that our algorithm improves the success rates of task satisfaction over both infinite and finite horizons in complex environments, and significantly reduces training time for the task over finite horizons. Detailed descriptions of environments and LTL tasks will be introduced.

Baseline Approaches: We refer to our distributed framework as "RRT*" or "D-RRT*", and compare it against three baselines: (i) The TL-based rewards in [26], [28] referred as "TL", for the single LTL task, have shown excellent performance in non-complex environments, which generalizes the cases of finite horizons in existing literature [23]–[25]; (ii) Similar as [38], [39], for the goal-reaching task ϕ , the baseline referred to as "NED" designs the reward based on the negative Euclidean distance between the robot and destination; (iii) For a complex LTL task, instead of decomposition, this baseline directly apply the reward scheme (3) for the global trajectory $\tau_F^* = \tau_{pre}^*[\tau_{suf}^*]^\omega$ referred as "G-RRT*". Note that we focus on comparing the baseline "NED" for finite-horizon tasks and the baseline "G-RRT*" for infinite-horizon and complex tasks.

6.1 Autonomous Vehicle We first implement the car-like model of Pybullet¹ physical engine shown in Fig. 3. We consider the sequential LTL task and surveillance LTL task over both finite and infinite horizons as $\phi_{2,fin} = \square \neg \mathcal{O} \wedge \diamond (\mathcal{G}_1 \wedge \diamond (\mathcal{G}_2 \wedge \diamond (\mathcal{G}_3 \wedge \diamond \mathcal{G}_{init})))$ and $\phi_{2,inf} = \square \neg \mathcal{O} \wedge \square \diamond (\mathcal{G}_1 \wedge \diamond (\mathcal{G}_2 \wedge \diamond (\mathcal{G}_3)))$, respectively, where $\phi_{2,fin}$ requires the vehicle to visit goal regions labeled as $\mathcal{G}_1, \mathcal{G}_2, \mathcal{G}_3$ and initial position sequentially, and $\phi_{1,inf}$ requires to visit initial positions and other goal regions infinitely often. Fig. 3 (a) and (b) show the learning curves of task $\phi_{2,fin}$ and $\phi_{2,inf}$, respectively, compared with different baselines. We can observe

¹<https://pybullet.org/wordpress/>

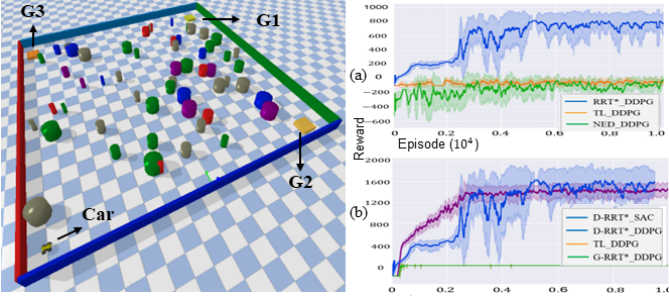


Fig. 3. Baselines comparison of tasks $\phi_{2,fin}$ (a) and $\phi_{2,inf}$ (b) in the Pybullet environment.

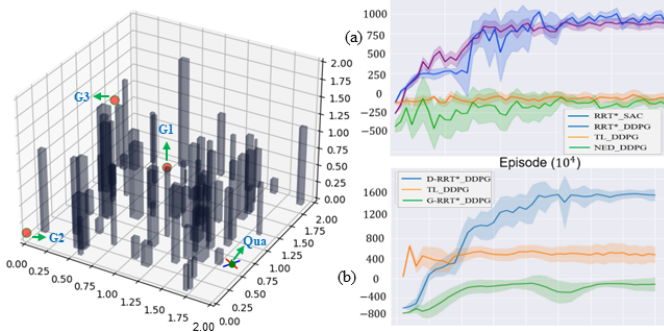


Fig. 4. Baselines comparison of tasks $\phi_{1,fin}$ in (a) and $\phi_{1,inf}$ in (b) of the complex 3D quadrotor environment.

that our framework can be adopted in both DDPG and SAC to provide better performance than other baselines in complex cluttered environments.

6.2 Quadrotor Model We implement our algorithms in a 3D environment with Quadrotor² dynamics shown in Fig. 4, which shows the capability of handling complex cluttered environments and high dimensional systems. We also test two types of LTL specifications as $\phi_{1,fin} = \square \neg \mathcal{O} \wedge \diamond \mathcal{G}_1 \wedge \diamond \mathcal{G}_2 \wedge \diamond \mathcal{G}_3$ and $\phi_{1,inf} = \square \neg \mathcal{O} \wedge \square \diamond \mathcal{G}_1 \wedge \square \diamond \mathcal{G}_2 \wedge \square \diamond \mathcal{G}_3$. The learning results for these tasks are shown in Fig 4 (a) and (b), respectively, which shows the state-of-art of our framework.

Then, we increase the complexity by random sampling 12 obstacle-free goal regions in the 3D environment and set the rich specifications as $\phi_{3,fin} = \square \neg \mathcal{O} \wedge ((\diamond \mathcal{G}_1 \wedge \diamond (\mathcal{G}_2 \wedge \diamond \dots \wedge \diamond \mathcal{G}_{12})))$, and $\phi_{3,inf} = \square \neg \mathcal{O} \wedge \square \diamond \mathcal{G}_1 \wedge \square \diamond \mathcal{G}_2 \dots \wedge \square \diamond \mathcal{G}_{12}$. The results are shown in Fig. 5 (a) and (b), and we observe that the "TL" baseline is sensitive to the environments and has poor performances, and when the optimal trajectories become complicated in the sense of the complexity of LTL tasks, "G-RRT*" easily converge to the sub-optimal solutions.

6.3 Performance Evaluation Since our algorithm learns to complete the task faster, that terminates each episode during learning earlier for tasks over finite horizons. To illustrate the efficiency, we implement the training process 10 times for tasks ϕ , $\phi_{1,fin}$, $\phi_{2,fin}$, $\phi_{3,fin}$ in both complex cluttered environments and dynamics, and record the average training time compared with the baseline modular "TL" [26] and distributed "NED" (D-NED). The results in Fig. 5 (d) show that

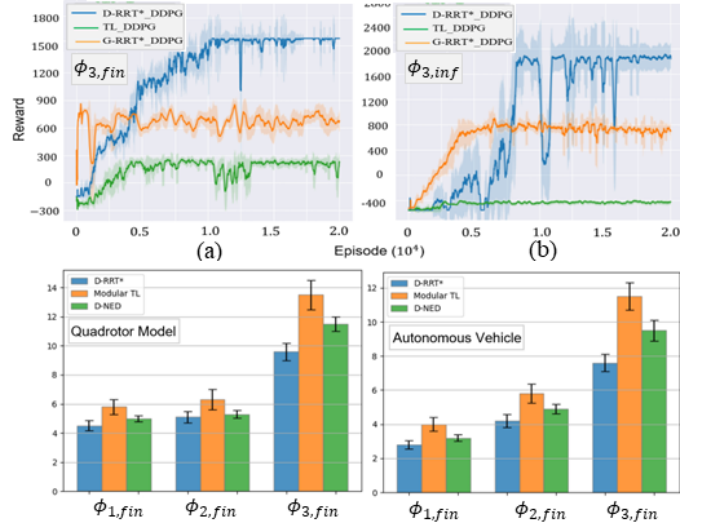


Fig. 5. (a) (b) Results of baselines for more complex task $\phi_{3,fin}$ and $\phi_{3,inf}$ in complex 3D environments; (d) Training time comparison for all tasks over finite horizons in both environments and dynamic systems.

TABLE I
ANALYSIS OF SUCCESS RATES AND TRAINING TIME.

LTL Task	Dynamic model	Baseline rate	Success rate
$\phi_{1,fin}$	Quadrotor	D-RRT*	100%
		TL, G-RRT*	0%
$\phi_{2,fin}$	Vehicle	D-RRT*	100%
		TL, G-RRT*	0%
$\phi_{3,fin}$	Quadrotor	D-RRT*	100%
		TL, G-RRT*	0%
$\phi_{3,fin}$	Vehicle	D-RRT*	100%
		TL, G-RRT*	0%
$\phi_{1,inf}$	Quadrotor	D-RRT*	100%
		TL, G-RRT*	0%
$\phi_{2,inf}$	Vehicle	D-RRT*	100%
		TL, G-RRT*	0%
$\phi_{3,inf}$	Quadrotor	D-RRT*	100%
		TL, G-RRT*	0%
$\phi_{3,inf}$	Vehicle	D-RRT*	100%
		TL, G-RRT*	0%

we have optimized the learning efficiency and the training time is reduced. In practice, we can apply distributed computing to train each local DPG of sub-tasks simultaneously for complicated global tasks to alleviate the training burden.

We statistically run 200 trials of the learned policies for each sub-task and record the average success rates and training time of both models, i.e., autonomous vehicle and quadrotor. The results are shown in Table I. We see that in complex environments, success rates of other all baselines are 0, and our method achieves success rates of near 100%. As a result, the effectiveness of the performance has been significantly improved under environmental challenges.

VII. CONCLUSION

Applying DPG algorithms to complex environments produces vastly different behaviors and results in failure to complete

²<https://github.com/Bharath2/Quadrotor-Simulation/tree/main/PathPlanning>

complex tasks. A persistent problem is the exploration phase of the learning process and the density of reward designs that limit its applications to real-world robotic systems. This paper provides a novel path-planning-based reward scheme to alleviate this problem, enabling significant improvement of reward performance and generating optimal policies satisfying complex specifications in complex cluttered environments. To facilitate rich high-level specification, we develop an optimal decomposition strategy for the global LTL task, allowing to train all sub-tasks in parallel and optimize the efficiency. The main limitation of our approach is to generalize various environments from a distribution. Future works aim at shrinking the gap of sim-to-real. We will also consider safety-critical exploration during learning and investigate multi-agent systems.

REFERENCES

- [1] V. Mnih, K. Kavukcuoglu, D. Silver, A. A. Rusu, J. Veness, M. G. Bellemare, A. Graves, M. Riedmiller, A. K. Fidjeland, G. Ostrovski *et al.*, “Human-level control through deep reinforcement learning,” *nature*, vol. 518, no. 7540, pp. 529–533, 2015.
- [2] R. S. Sutton and A. G. Barto, *Reinforcement learning: An introduction*. MIT press, 2018.
- [3] J. Schulman, S. Levine, P. Abbeel, M. Jordan, and P. Moritz, “Trust region policy optimization,” in *International conference on machine learning*. PMLR, 2015, pp. 1889–1897.
- [4] T. P. Lillicrap, J. J. Hunt, A. Pritzel, N. Heess, T. Erez, Y. Tassa, D. Silver, and D. Wierstra, “Continuous control with deep reinforcement learning,” *arXiv preprint arXiv:1509.02971*, 2015.
- [5] J. Schulman, F. Wolski, P. Dhariwal, A. Radford, and O. Klimov, “Proximal policy optimization algorithms,” *OpenAI*, 2017.
- [6] R. Lowe, Y. Wu, A. Tamar, J. Harb, P. Abbeel, and I. Mordatch, “Multi-agent actor-critic for mixed cooperative-competitive environments,” *Advances in Neural Information Processing Systems (NeurIPS)*, 2017.
- [7] T. Haarnoja, A. Zhou, P. Abbeel, and S. Levine, “Soft actor-critic: Off-policy maximum entropy deep reinforcement learning with a stochastic actor,” in *International conference on machine learning*. PMLR, 2018, pp. 1861–1870.
- [8] T. Hester, M. Vecerik, O. Pietquin, M. Lanctot, T. Schaul, B. Piot, D. Horgan, J. Quan, A. Sendonaris, I. Osband *et al.*, “Deep q-learning from demonstrations,” in *Thirty-second AAAI conference on artificial intelligence*, 2018.
- [9] A. Nair, B. McGrew, M. Andrychowicz, W. Zaremba, and P. Abbeel, “Overcoming exploration in reinforcement learning with demonstrations,” in *2018 IEEE International Conference on Robotics and Automation (ICRA)*. IEEE, 2018, pp. 6292–6299.
- [10] M. Vecerik, T. Hester, J. Scholz, F. Wang, O. Pietquin, B. Piot, N. Heess, T. Rothörl, T. Lampe, and M. Riedmiller, “Leveraging demonstrations for deep reinforcement learning on robotics problems with sparse rewards,” *arXiv preprint arXiv:1707.08817*, 2017.
- [11] S. Fujimoto, D. Meger, and D. Precup, “Off-policy deep reinforcement learning without exploration,” in *International Conference on Machine Learning*. PMLR, 2019, pp. 2052–2062.
- [12] S. M. LaValle and J. J. Kuffner Jr, “Randomized kinodynamic planning,” *The international journal of robotics research*, vol. 20, no. 5, pp. 378–400, 2001.
- [13] S. Karaman and E. Frazzoli, “Sampling-based algorithms for optimal motion planning,” *The international journal of robotics research*, vol. 30, no. 7, pp. 846–894, 2011.
- [14] S. M. LaValle, M. S. Branicky, and S. R. Lindemann, “On the relationship between classical grid search and probabilistic roadmaps,” *The International Journal of Robotics Research*, vol. 23, no. 7-8, pp. 673–692, 2004.
- [15] S. J. Qin and T. A. Badgwell, “A survey of industrial model predictive control technology,” *Control engineering practice*, vol. 11, no. 7, pp. 733–764, 2003.
- [16] I. R. Manchester and J.-J. E. Slotine, “Control contraction metrics: Convex and intrinsic criteria for nonlinear feedback design,” *IEEE Transactions on Automatic Control*, vol. 62, no. 6, pp. 3046–3053, 2017.
- [17] C. Dawson, Z. Qin, S. Gao, and C. Fan, “Safe nonlinear control using robust neural lyapunov-barrier functions,” in *Conference on Robot Learning*. PMLR, 2022, pp. 1724–1735.
- [18] C. Baier and J.-P. Katoen, *Principles of model checking*. MIT press, 2008.
- [19] R. T. Icarte, T. Klassen, R. Valenzano, and S. McIlraith, “Using reward machines for high-level task specification and decomposition in reinforcement learning,” in *International Conference on Machine Learning*, 2018, pp. 2107–2116.
- [20] A. Camacho, R. T. Icarte, T. Q. Klassen, R. A. Valenzano, and S. A. McIlraith, “LTL and beyond: Formal languages for reward function specification in reinforcement learning,” in *IJCAI*, vol. 19, 2019, pp. 6065–6073.
- [21] M. Hasanbeig, N. Y. Jeppu, A. Abate, T. Melham, and D. Kroening, “Deepsynth: Program synthesis for automatic task segmentation in deep reinforcement learning,” in *Proceedings of the AAAI Conference on Artificial Intelligence*, 2019.
- [22] Z. Xu, I. Gavran, Y. Ahmad, R. Majumdar, D. Neider, U. Topcu, and B. Wu, “Joint inference of reward machines and policies for reinforcement learning,” in *Proceedings of the International Conference on Automated Planning and Scheduling*, vol. 30, 2020, pp. 590–598.
- [23] X. Li, Z. Serlin, G. Yang, and C. Belta, “A formal methods approach to interpretable reinforcement learning for robotic planning,” *Science Robotics*, vol. 4, no. 37, 2019.
- [24] P. Vaezipoor, A. Li, R. T. Icarte, and S. McIlraith, “Ltl2action: Generalizing ltl instructions for multi-task rl,” *International Conference on Machine Learning, PMLR*, 2021.
- [25] R. T. Icarte, T. Q. Klassen, R. Valenzano, and S. A. McIlraith, “Reward machines: Exploiting reward function structure in reinforcement learning,” *Journal of Artificial Intelligence Research*, vol. 73, pp. 173–208, 2022.
- [26] M. Cai, M. Hasanbeig, S. Xiao, A. Abate, and Z. Kan, “Modular deep reinforcement learning for continuous motion planning with temporal logic,” *IEEE Robotics and Automation Letters*, vol. 6, no. 4, pp. 7973–7980, 2021.
- [27] M. Cai and C.-I. Vasile, “Safety-critical modular deep reinforcement learning with temporal logic through gaussian processes and control barrier functions,” *arXiv preprint arXiv:2109.02791*, 2021.
- [28] M. Hasanbeig, D. Kroening, and A. Abate, “Deep reinforcement learning with temporal logics,” in *International Conference on Formal Modeling and Analysis of Timed Systems*. Springer, 2020, pp. 1–22.
- [29] S. Sickert, J. Esparza, S. Jaax, and J. Křetínský, “Limit-deterministic Büchi automata for linear temporal logic,” in *Int. Conf. Comput. Aided Verif.* Springer, 2016, pp. 312–332.
- [30] C. I. Vasile, X. Li, and C. Belta, “Reactive sampling-based path planning with temporal logic specifications,” *The International Journal of Robotics Research*, vol. 39, no. 8, pp. 1002–1028, 2020.
- [31] Y. Kantaros and M. M. Zavlanos, “Stylus*: A temporal logic optimal control synthesis algorithm for large-scale multi-robot systems,” *The International Journal of Robotics Research*, vol. 39, no. 7, pp. 812–836, 2020.
- [32] M. Srinivasan and S. Coogan, “Control of mobile robots using barrier functions under temporal logic specifications,” *IEEE Transactions on Robotics*, vol. 37, no. 2, pp. 363–374, 2020.
- [33] X. Luo, Y. Kantaros, and M. M. Zavlanos, “An abstraction-free method for multirobot temporal logic optimal control synthesis,” *IEEE Transactions on Robotics*, 2021.
- [34] S. Thrun, “Probabilistic robotics,” *Communications of the ACM*, vol. 45, no. 3, pp. 52–57, 2002.
- [35] M. Kloetzer and C. Belta, “A fully automated framework for control of linear systems from temporal logic specifications,” *IEEE Transactions on Automatic Control*, vol. 53, no. 1, pp. 287–297, 2008.
- [36] M. Y. Vardi and P. Wolper, “An automata-theoretic approach to automatic program verification,” in *Proceedings of the First Symposium on Logic in Computer Science*. IEEE Computer Society, 1986, pp. 322–331.
- [37] P. Gastin and D. Oddoux, “Fast ltl to büchi automata translation,” in *International Conference on Computer Aided Verification*. Springer, 2001, pp. 53–65.
- [38] P. Long, T. Fan, X. Liao, W. Liu, H. Zhang, and J. Pan, “Towards optimally decentralized multi-robot collision avoidance via deep reinforcement learning,” in *2018 IEEE International Conference on Robotics and Automation (ICRA)*. IEEE, 2018, pp. 6252–6259.
- [39] C. Dawson, B. Lowenkamp, D. Goff, and C. Fan, “Learning safe, generalizable perception-based hybrid control with certificates,” *IEEE Robotics and Automation Letters*, vol. 7, no. 2, pp. 1904–1911, 2022.
- [40] R. Durrett and R. Durrett, *Essentials of stochastic processes*. Springer, 1999, vol. 1.

APPENDIX

A. Summary of Geometric RRT*

Before discussing the algorithm in details, it is necessary to introduce few algorithmic primitives as follows:

Random sampling: The *Sample* function provides independent, uniformly distributed random samples of states, from the geometric space X .

Distance and cost: The function $dist : X \times X \rightarrow [0, \infty)$ is the metric that returns the geometric Euclidean distance. The function $Cost : X \rightarrow [0, \infty)$ returns the length of the path from the initial state x_0 to the input state.

Nearest neighbor: Given a set of vertices V in the tree G and a state x' , the function $Nearest(V, x)$ generates the closest state $x \in V$ from which x' can be reached with the lowest distance metric.

Steering: Given two states x, x' , the function *Steer* returns a state x_{new} such that x_{new} lies on the geometric line connecting x to x' , and its distance from x is at most η , i.e., $dist(x, x') \leq \eta$, where η is a user-specified parameter. In addition, the state x_{new} must satisfy $dist(x_{new}, x') \leq dist(x, x')$. The function *Steer* also returns the straight line σ connecting x to x_{new} .

Collision check: A function $CollisionFree(\sigma)$ that detects if a state trajectory σ lies in the obstacle-free portion of space X . $C(\sigma)$ is the distance of σ .

Near nodes: Given a set of vertices V in the tree G and a state x' , the function $Near(V, x')$ returns a set of states that are closer than a threshold cost to x' :

$$Near(V, x') = \left\{ x \in V : dist(x, x') \leq \kappa \left(\frac{\log n}{n} \right)^{1/d} \right\},$$

where n is the number of vertices in the tree, d is the dimension of the geometric space, and κ is a constant.

Optimal Path: Given two states x, x' in V , the function $Path(x, x')$ returns a local optimal trajectory σ .

The Alg. 2 proceeds as follows. First, the graph G is initialized with $V \leftarrow \{x_0\}$ and $E \leftarrow \emptyset$ (line 1). Then a state x_{rand} is sampled from X of Env (line 3), then, the nearest node $x_{nearest}$ in the tree is found (line 4) and extended toward the sample, denoted by x_{new} , in addition to the straight line σ_{new} connecting them (line 5). If line σ_{new} is collision free (line 6), the algorithm iterates over all near neighbors of the state x_{new} and finds the state x_{min} that has the lowest cost to reach x_{new} (lines 7- 15). Then the tree is updated with the new state (lines 16- 17), and the algorithm rewires the near nodes, using Alg. 3 (line 18). Alg. 3 iterates over the near neighbors of the new state x_{new} and updates the parent of a near state x_{near} to x_{new} if the cost of reaching x_{near} from x_{new} is less than the current cost of reaching to x_{near} .

B. Analysis of Product State

In this section, we show that the product state can be applied with RL algorithms and the (3) is a Markovian reward for the state $s^\times = (s_t, i_t)$. Let $I = \{0, 1, \dots, N_p\}$ be a set of all sequential indexes of the r-balls for an optimal trajectory x^* , and define $f_I : \mathbb{R} \rightarrow I$ as function to return the index at each

Algorithm 2 Geometric RRT* $((V, E), N)$

```

1: Initialize:  $G = (V, E); V \leftarrow \{x_0\}, E \leftarrow \emptyset$ 
2: for  $i = 1, \dots, N$  do
3:    $x_{rand} \leftarrow Sample$ 
4:    $x_{nearest} \leftarrow Nearest(V, x_{rand})$ 
5:    $x_{new}, \sigma_{new} \leftarrow Steer(x_{nearest}, x_{rand})$ 
6:   if  $CollisionFree(\sigma_{new})$  then
7:      $X_{near} \leftarrow Near(V, x_{new})$ 
8:      $c_{min} \leftarrow \infty, x_{min} \leftarrow NULL, \sigma_{min} \leftarrow NULL$ 
9:     for  $x_{near} \in X_{near}$  do
10:       $\sigma \leftarrow Path(x_{near}, x_{new})$ 
11:      if  $Cost(x_{near}) + C(z) < c_{min}$  then
12:         $c_{min} \leftarrow Cost(x_{near}) + Cost(\sigma)$ 
13:         $x_{min} \leftarrow x_{near}; \sigma_{min} \leftarrow \sigma$ 
14:      end if
15:    end for
16:     $V \leftarrow V \cup \{x_{new}\}$ 
17:     $E \leftarrow E \cup \{(x_{min}, x_{new})\}$ 
18:     $(V, E) \leftarrow Rewire((V, E), X_{near}, x_{new})$ 
19:  end if
20: end for
21: return  $G = (V, E)$ 

```

Algorithm 3 Rewire $((V, E), X_{near}, x_{new})$

```

1: for  $x_{near} \in X_{near}$  do
2:    $\sigma \leftarrow Path(x_{new}, x_{near})$ 
3:   if  $Cost(x_{new}) + C(\sigma) < Cost(x_{near})$  then
4:     if  $CollisionFree(x)$  then
5:        $x_{parent} \leftarrow Parent(x_{near})$ 
6:        $E \leftarrow E \setminus \{(x_{parent}, x_{near})\}$ 
7:        $E \leftarrow E \cup \{(x_{new}, x_{near})\}$ 
8:     end if
9:   end if
10: end for
11: return  $G = (V, E)$ 

```

time t s.t. $f_I(t) = i_t$, where the output of the function f_I follows the requirements:

$$\begin{cases} i_t = 0, & \text{if none of the r-balls are visited up to } t, \\ x_{i_t} = Proj(s_{i_t}), & \text{where } s_{i_t} = \arg \min_{s \in s_t} \{D(Proj(s))\}. \end{cases}$$

Consequently, given an input t , the f_I generates a deterministic output such that we regard the tuple (I, f_I, i_0) as a deterministic automaton without accepting states [18], where $i_0 = 0$. The state s_t^\times is derived from a product structure defined as:

Definition 4. The product between cl-MPD $\mathcal{M} = (S, S_0, A, p_S, AP, L, R, \gamma)$ and (I, f_I, i_0) is a tuple $\mathcal{M}^\times = (S^\times, S_0^\times, A, p_S^\times, AP, L^\times, R, \gamma)$, where $S^\times = S \times I$ is a set of product states; $S_0^\times = S_0 \times i_0$ is a set of initial states; p_S^\times is the transition distribution s.t. for states $(s^\times = (s, i), (s'^\times = (s', i'))$, $p_S^\times(s'^\times | s^\times, a) > 0$ iff $p_S(s' | s, a) > 0$, $a \in A$ and $i' = f_I(i)$; $L^\times(s^\times = L(s), \forall s^\times = (s, i)$.

According to [18], \mathcal{M}^\times is a product MDP structure that allows using RL methods to find the optimal policy, where the state i_t of s_t^\times tracks the history of state trajectory s_{t-1} up to t .

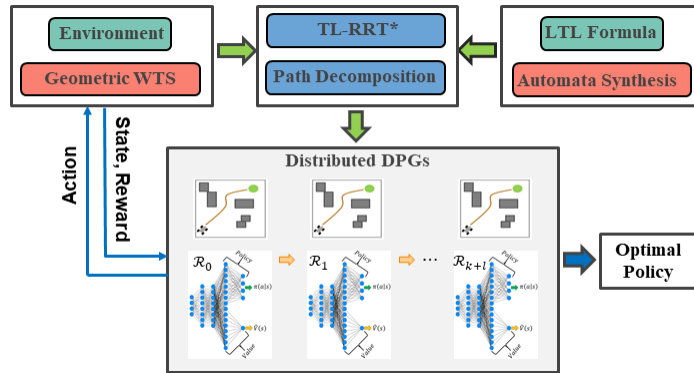


Fig. 6. General diagram of the LTL-RRT*-Distributed DPGs method explained in Alg. 1.

Consequently, the reward (3) is a Markovian reward function.

C. Theorem 1 Proof

First, we introduce two relevant definitions:

Definition 5. [18] A Markov chain $MC_{\mathcal{P}}^{\pi}$ of the \mathcal{M} is a sub-MDP of \mathcal{M} induced by a policy π .

Definition 6. [40] States of any Markov chain $MC_{\mathcal{P}}^{\pi}$ under policy π are represented by a disjoint union of a transient class $T(\pi)$ and n_R closed irreducible recurrent classes $Re^j(\pi)$, $j \in \{1, \dots, n_{Re}\}$, where a class is a set of states. That is, for any policy π , one has

$$MC_{\mathcal{P}}^{\pi} = Tr(\pi) \sqcup Re^1(\pi) \sqcup Re^2(\pi) \sqcup \dots \sqcup Re^{n_{Re}}(\pi).$$

As discussed in [40], for each state in recurrent class, it holds that $\sum_{n=0}^{\infty} p^n(s^{\times}, s^{\times}) = \infty$, where $s^{\times} \in R_{\pi}^j \cap F_k^{\mathcal{P}}$ and $p^n(s^{\times}, s^{\times})$ denotes the probability of returning from a transient state s^{\times} to itself in n steps. This means that each state in the recurrent class occurs infinitely often.

Then, we prove it by the contradiction. Suppose we have a policy $\bar{\pi}$ that is optimal and does not satisfy go-reach task ϕ_p , which means the robot derived by $\bar{\pi}$ will not reach the goal station. According to the reward design (3), the robot is only assigned repetitive reward R_{++} when it reaches and stays at the destination s.t. $D(Proj(s_t)) = 0$. We have that rewards of states in recurrent classes are equal zero i.e., $R(s_t^{\times}) = 0, \forall s_t^{\times} \in Re^j(\bar{\pi}), \forall j \in \{1, \dots, n_{Re}\}$. Recall that we have N_p r-balls, and the best case of $\bar{\pi}$ is to consecutively pass all these balls sequentially without reaching destination. We obtain the upper-bound of $J(\bar{\pi})$ as:

$$J(\bar{\pi}) < R_{++} \cdot \frac{1 - \gamma^{N_p}}{1 - \gamma} \quad (7)$$

Per assumption 1, we can find another policy π^* that reaches and stays at the destination s.t. $R(s_t^{\times}) = R_{++}, \forall s_t^{\times} \in Re^j(\pi^*), \forall j \in \{1, \dots, n_{Re}\}$. The worst case of π^* is to pass no r-balls in the class $Tr(\bar{\pi})$ and only reach the goal stations. We obtain the lower-bound of $J(\pi^*)$ as:

$$J(\pi^*) \geq \underline{M}R_{++} \cdot \frac{1}{1 - \gamma}, \quad (8)$$

where $\underline{M} = \gamma^{\bar{n}}$, and \bar{n} is maximum number of steps reaching the goal station region. Consequently, for (7) and (8), if we select

$$R_{++} \geq \frac{R_{+} \cdot (1 - \gamma^{N_p})}{\underline{M}}, \quad (9)$$

we guarantee that $J(\pi^*) > J(\bar{\pi})$, which contradicts the fact that $\bar{\pi}$ is an optimal policy. This concludes the theorem.

Note that, the above proof only considers the worst case of optimal policies satisfying goal-reaching task ϕ_p . According to the design of the RRT* reward (2), in practice, we can achieve better convergence due to the high density of r-balls in geometric space.

D. Diagram for Alg. 1

Here we present a general diagram of our proposed method in Alg. 1. From the given environment Env with geometric space X , the G-WTS \mathcal{T} is constructed. This transition system, together with the NBA \mathcal{B} generated from the LTL task ϕ_{p2} , are used to construct the PBA P . The TL-RRT* method is applied over P to compute the optimal accepting run τ_F^* and the optimal trajectory R_F^* . Using the path decomposition with respect to the order of segments in (5), distributed DPGs are trained in parallel over the episodes, and the resulting optimal distributed policies are concatenated sequentially to satisfy the LTL formula in the form of ϕ_{p2} . Based on the decomposition properties, we have:

Lemma 1. *If Assumption 1 holds, by selecting R_{++} to be sufficiently larger than R_{+} , i.e., $R_{++} \gg R_{+}$, Alg. 1 using a suitable DPG algorithm can generate the optimal policy $\pi_{\theta}^* = (\pi_0^* \pi_1^* \dots \pi_K^*)(\pi_{K+1}^* \dots \pi_{K+l}^*)^{\omega}$ satisfying the general LTL task ϕ_{p2} , i.e., $\Pr_{\pi_M^*}(\phi_{p2}) > 0$ in the limit.*

Proof. Since the TL-RRT* [33] has shown to find the optimal geometric path to satisfy ϕ_{p2} , which is decomposed into sub-tasks in the form of $\mathcal{R}_F^* = (\mathcal{R}_0 \mathcal{R}_1 \dots \mathcal{R}_K)(\mathcal{R}_{K+1} \dots \mathcal{R}_{K+l})^{\omega}$, from Theorem 2, each optimal sub-policy π_i^* achieves the sub-task of \mathcal{R}_i . This concludes Lemma 1. Note that the LTL formula ϕ is a special case of ϕ_{p2} that only has one DPG for training and is solved via Alg. 1. \square

E. Experimental Setting

All experiments are conducted on a 16GB computer using 1 Nvidia RTX 3060 GPU. In each experiment, the LTL tasks are converted into NBA using the tool: <http://www.lsv.fr/~gastin/ltl2ba/>. The cl-MDP between the dynamic system and environmental geometric space is synthesized on-the-fly. The parameters of the reward scheme are set as $R_- \in \{-100, -200\}$, $R_{++} = 200$, $R_+ = 5$.

We run 10000 episodes for the task $\phi_{2,inf}, \phi_{2,fin}$, 20000 episodes for the tasks $\phi_{1,inf}, \phi_{1,fin}, \phi_{3,inf}, \phi_{3,fin}$. Every episode has maximum 1000 steps for tasks $\phi_{1,inf}, \phi_{1,fin}, \phi_{2,inf}, \phi_{2,fin}$, and each episode of the tasks $\phi_{3,inf}, \phi_{3,fin}$ has maximum 1500 steps.

As for each actor/critic structure, we use the same feed-forward neural network setting with 3 fully connected layers with [64, 64, 64] units and the ReLU activation function. We use the implementations of DDPG and PPO for tuning parameters according to the OpenAI baselines: <https://github.com/openai/baselines>.